

Reti-Diff: Illumination Degradation Image Restoration with Retinex-based Latent Diffusion Model

Chunming He^{1,*}, Chengyu Fang^{1,*}, Yulun Zhang^{2,†}, Kai Li³,
Longxiang Tang¹, Chenyu You⁴, Fengyang Xiao⁵, Zhenhua Guo⁶, and Xiu Li^{1,†}

¹Shenzhen International Graduate School, Tsinghua University, ²ETH Zürich,
³NEC Laboratories America, ⁴Yale University, ⁵Sun Yat-Sen University, ⁶Tianyi Traffic Technology

Abstract

Illumination degradation image restoration (IDIR) techniques aim to improve the visibility of degraded images and mitigate the adverse effects of deteriorated illumination. Among these algorithms, diffusion model (DM)-based methods have shown promising performance but are often burdened by heavy computational demands and pixel misalignment issues when predicting the image-level distribution. To tackle these problems, we propose to leverage DM within a compact latent space to generate concise guidance priors and introduce a novel solution called Reti-Diff for the IDIR task. Reti-Diff comprises two key components: the Retinex-based latent DM (RLDM) and the Retinex-guided transformer (RGformer). To ensure detailed reconstruction and illumination correction, RLDM is empowered to acquire Retinex knowledge and extract reflectance and illumination priors. These priors are subsequently utilized by RGformer to guide the decomposition of image features into their respective reflectance and illumination components. Following this, RGformer further enhances and consolidates the decomposed features, resulting in the production of refined images with consistent content and robustness to handle complex degradation scenarios. Extensive experiments show that Reti-Diff outperforms existing methods on three IDIR tasks, as well as downstream applications. Code will be available at <https://github.com/ChunmingHe/Reti-Diff>.

1. Introduction

Illumination degradation image restoration (IDIR) seeks to enhance the visibility and contrast of degraded images while mitigating the adverse effects of deteriorated illumination, e.g., indefinite noise and variable color deviation. IDIR has been investigated in various domains, including low-light image enhancement [2]. By addressing illumi-

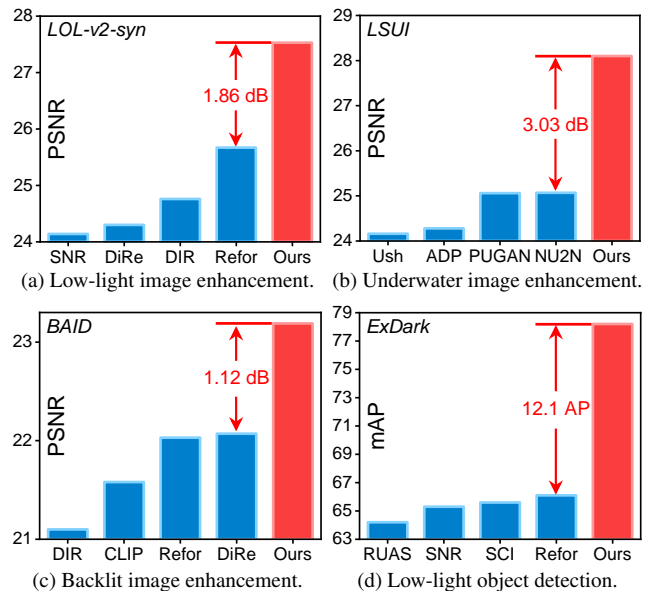


Figure 1. Our Reti-Diff outperforms cutting-edge techniques including RUAS [33], SNR (SNR-Net [57]), SCI [42], Ush (U-shape [47]), PUGAN [7], ADP [69], NU2Net [15], DiRe (Diff-Retinex [62]), DIR (DiffIR [55]), ReFor (RetFormer [2]), CLIP (CLIP-LIT [32]) in three IDIR tasks with three benchmarks: *LOL-v2-syn* [61], *LSUI* [47], and *BAID* [40]. We also verify our superiority on low-light object detection with the *ExDark* [36] dataset.

nation degradation, the enhanced images are expected to exhibit improved visual quality, making them more suitable for decision-making or subsequent tasks like nighttime object detection and segmentation. underwater image enhancement [15], and backlit image enhancement [32].

Traditional IDIR approaches [12, 49] primarily rely on manually crafted enhancement techniques with limited generalization capabilities. Leveraging the robust feature extraction capabilities of convolutional neural networks and transformers, a series of deep learning-based methods [2, 24] have been proposed and have achieved remarkable success in the IDIR domain. However, as depicted in Fig. 1,

*Equal Contribution, † Corresponding Author

they still face challenges in complex illumination degradation scenarios due to their constrained generative capacity.

To overcome these challenges, deep generative models, like generative adversarial networks [16] and variational autoencoder [8], have gained popularity for addressing the IDIR problem, owing to their potent generative abilities. Recently, the diffusion model (DM) [62] has been introduced to the IDIR field for high-quality image restoration, as it offers accurate results without mode collapse, a common issue with other generative models. However, the existing DM-based method, Diff-Retinex [62], applies DM directly to image-level generation, leading to two main challenges: (1) This method incurs high computational costs, as predicting the image-level distribution requires a large number of inference steps. (2) The enhanced results may exhibit pixel misalignment with the original clean image in terms of restored details [5], resulting in suboptimal performance in distortion-based metrics like PSNR. Nevertheless, this issue can be effectively addressed by transformer-based methods, which excel in modeling long-range dependencies.

To tackle the aforementioned problems, we propose introducing the latent diffusion model (LDM) to address the IDIR problem. By applying DM in the low-dimensional compact latent space, we effectively alleviate the computational burden. Additionally, we incorporate LDM into transformers to prevent pixel misalignment in the generated image, which is often observed in existing deep generative models. Unlike existing LDM-based methods that solely use the priors extracted from the RGB domain, our method allows LDM to learn Retinex information from the reflectance and illumination domains, which are decomposed from the RGB domain. This approach enables us to simultaneously enhance image details using the reflectance prior and correct color distortions with the illumination prior, thereby improving illumination degradation.

With this inspiration, we propose the first LDM-based solution, Reti-Diff, to solve the IDIR problem. As shown in Fig. 2, Reti-Diff comprises two main parts: the Retinex-based LDM (RLDM) and the Retinex-guided transformer (RGformer). Initially, RLDM is employed to generate Retinex priors, which are then integrated into RGformer to produce visually appealing results. Following a common training strategy [55], we propose a two-phase approach, where we first pretrain Reti-Diff and subsequently optimize RLDM. **In phase I**, we introduce a Retinex prior extraction (RPE) module to compress the ground-truth image into the highly compact Retinex priors, specifically the reflectance prior and the illumination prior. These priors are then sent to RGformer to guide feature decomposition and the generation of reflectance and illumination features. Afterward, RGformer employs the Retinex-guided multi-head cross attention (RG-MCA) and dynamic feature aggregation (DFA) module to refine and aggregate the de-

composed features, ultimately producing enhanced images with coherent content and ensuring robustness and generalization in extreme degradation scenarios. **In phase II**, we train RLDM in reflectance and illumination domains to directly estimate Retinex priors from the degraded image, enhancing the quality of the generated priors and further improving reconstruction quality when jointly optimized with RGformer. Our contributions are summarized as follows:

- We propose a novel DM-based framework, Reti-Diff, for the IDIR task. To the best of our knowledge, this is the first application of the latent diffusion model to tackle the IDIR problem.
- We propose to let RLDM learn Retinex knowledge and extract reflectance and illumination priors, thus facilitating detail restoration and illumination correction.
- We propose RGformer to integrate extracted Retinex priors to decompose features into reflectance and illumination components and then utilize RG-MCA and DFA to refine and aggregate the decomposed features, ensuring robustness and generalization in complex illumination degradation scenarios.
- Extensive experiments on three IDIR tasks verify our superiority to existing methods in terms of image quality and favorability in downstream applications, including object detection and segmentation.

2. Related Works

Illumination Degradation Image Restoration. Early IDIR methods can be broadly categorized into three main approaches: histogram equalization (HE) [1], gamma correction (GC) [22], and Retinex theory [28]. HE-based and GC-based methods focus on directly amplifying the low contrast regions but overlook illumination factors. Retinex-based variants [13, 31] propose the development of priors to constrain the solution space for reflectance and illumination maps. However, these methods still rely on hand-crafted priors, limiting their ability to generalize effectively.

With the rapid development of deep learning, approaches based on CNNs and transformers [2, 16, 24] have achieved remarkable success in IDIR. For instance, LLNet [37] proposed a sparse denoising structure to enhance illumination and suppress noise. DIE [50] integrated Retinex cues into a learning-based structure, presenting a one-stage Retinex-based solution for color correction. To enhance generative capacity, Diff-Retinex [62] introduced DM to the IDIR field by directly applying it to image-level generation. However, Diff-Retinex entails significant computational costs and may lead to pixel misalignment issues with the original input, particularly concerning restored image details.

Diffusion Models. Diffusion models (DMs) have demonstrated considerable success in various domains, including density estimation [26] and data generation [20]. Such

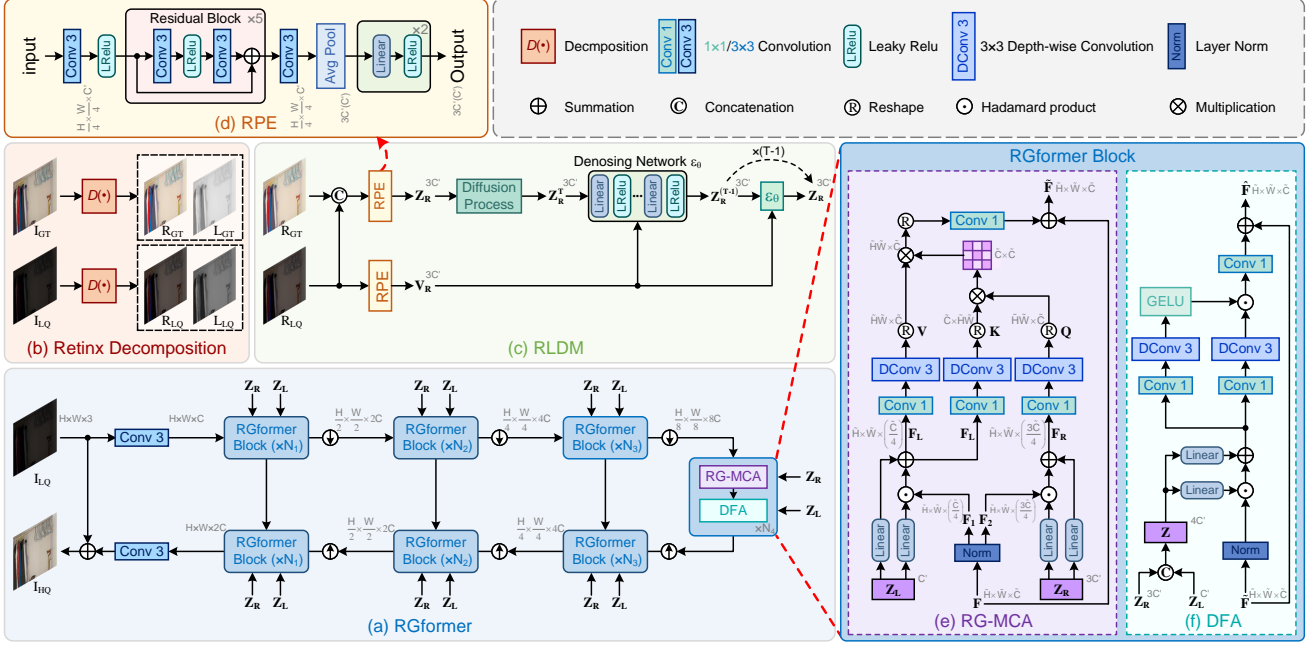


Figure 2. Framework of Reti-Diff. (a) consists of RG-MCA and DFA for image restoration, where we omit the auxiliary decoder $D_a(\cdot)$ for simplicity. In (c), we only give the example by using RLDM to extract the reflectance prior and the illumination prior is extracted similarly.

a probabilistic generative model adopts a parameterized Markov chain to optimize the lower variational bound on the likelihood function, enabling them to generate target distributions with greater accuracy than other generative models, *i.e.*, GAN and VAE. Recently, DMs have been introduced by Diff-Retinex [62] to solve the IDIR problem. However, when directly applied to image-level generation, this approach introduces computational burdens and issues related to pixel misalignment. To overcome this, we propose employing LDM to estimate priors within a low-dimensional latent space. We then integrate these priors into transformer-based restoration techniques, thus reducing the computational burden and preventing pixel misalignment. Besides, unlike existing LDM-based methods [5, 55] that solely rely on priors extracted from the RGB domain, our method allows LDM to acquire Retinex information from the reflectance and illumination domains. Therefore, this novel approach enables us to simultaneously enhance image details using the reflectance prior and correct color distortions with the illumination prior.

3. Methodology

In this paper, we leverage the latent diffusion model (LDM) to generate compact priors that guide illumination degradation image restoration (IDIR) tasks. This approach effectively reduces redundant computations and mitigates pixel misalignment issues often associated with traditional diffusion models (DM) [39, 62]. At the same time, it preserves the network’s generative capability, allowing it to address complex degradation scenarios. However, existing

LDM-based image restoration techniques [5, 55] primarily utilize priors extracted from the RGB domain for guidance, which limits their ability to fully exploit prior knowledge tailored to illumination degradation scenarios, ultimately impacting their restoration performance. In response to this challenge, we introduce Reti-Diff, which harnesses Retinex priors extracted from the illumination and reflectance domains to steer the image restoration process. By doing so, the extracted Retinex prior representation serves as dynamic modulation parameters, allowing for the simultaneous enhancement of restoration details via the reflectance prior and the correction of color distortion through the illumination prior. This ensures the generation of visually compelling results while favorably impacting downstream tasks.

As shown in Fig. 2, our Reti-Diff comprises two parts: the Retinex-guided transformer (RGformer) and the Retinex-based latent diffusion model (RLDM). Following [5, 55], Reti-Diff undergoes a two-phase training strategy, involving the initial pretraining of Reti-Diff and the subsequent optimization of RLDM. In this section, we provide an in-depth explanation of the two-phase training approach and illustrate the entire restoration process.

3.1. Pretrain Reti-Diff

We first pretrain Reti-Diff to encode the ground truth into compact priors with Retinex prior extraction (RPE) module and use them to guide RGformer for restoration.

Retinex prior extraction module. Given the low-quality (LQ) image $I_{LQ} \in \mathbb{R}^{H \times W \times 3}$ and its corresponding ground truth $I_{GT} \in \mathbb{R}^{H \times W \times 3}$, we initially decompose them into

the reflectance image $\mathbf{R} \in \mathbb{R}^{H \times W \times 3}$ and the illumination map $\mathbf{L} \in \mathbb{R}^{H \times W}$ according to Retinex theory:

$$\mathbf{I}_{LQ} = \mathbf{R}_{LQ} \odot \mathbf{L}_{LQ}, \mathbf{I}_{GT} = \mathbf{R}_{GT} \odot \mathbf{L}_{GT}, \quad (1)$$

where \odot denotes the Hadamard product. Following Retformer [2], We use a pretrained decomposing network $D(\cdot)$ to decompose \mathbf{I}_{LQ} and \mathbf{I}_{GT} . Then we concatenate $\text{conca}(\cdot)$ the corresponding components of ground truth and LQ image and use the RPE module $\text{RPE}(\cdot)$ to encode them into Retinex priors $\mathbf{Z}_R \in \mathbb{R}^{3C'}$, $\mathbf{Z}_L \in \mathbb{R}^{C'}$:

$$\begin{aligned} \mathbf{Z}_R &= \text{RPE}(\text{down}(\text{conca}(\mathbf{R}_{GT}, \mathbf{R}_{LQ}))), \\ \mathbf{Z}_L &= \text{RPE}(\text{down}(\text{conca}(\mathbf{L}_{GT}, \mathbf{L}_{LQ}))), \end{aligned} \quad (2)$$

where $\text{down}(\cdot)$ means downsampling and we use the PixelUnshuffle operation here. We then send Retinex priors, *i.e.*, \mathbf{Z}_R and \mathbf{Z}_L , to RGformer to serve as dynamic modulation parameters for detail restoration and color correction.

Retinex-guided transformer. RGformer mainly consists of two parts in each block, *i.e.*, Retinex-guided multi-head cross attention (RG-MCA) and dynamic feature aggregation (DFA) module. In RG-MCA, we first split the input feature $\mathbf{F} \in \mathbb{R}^{\tilde{H} \times \tilde{W} \times \tilde{C}}$ into two parts $\mathbf{F}_1 \in \mathbb{R}^{\tilde{H} \times \tilde{W} \times (3\tilde{C}/4)}$ and $\mathbf{F}_2 \in \mathbb{R}^{\tilde{H} \times \tilde{W} \times (\tilde{C}/4)}$ along the channel dimension. Afterwards, we integrated \mathbf{Z}_R and \mathbf{Z}_L as the corresponding dynamic modulation parameters to generate reflectance-guided feature $\mathbf{F}_R \in \mathbb{R}^{\tilde{H} \times \tilde{W} \times (3\tilde{C}/4)}$ and illumination-guided feature $\mathbf{F}_L \in \mathbb{R}^{\tilde{H} \times \tilde{W} \times (\tilde{C}/4)}$:

$$\begin{aligned} \mathbf{F}_R &= \text{Li}_1(\mathbf{Z}_R) \odot \text{Norm}(\mathbf{F}_1) + \text{Li}_2(\mathbf{Z}_R), \\ \mathbf{F}_L &= \text{Li}_1(\mathbf{Z}_L) \odot \text{Norm}(\mathbf{F}_2) + \text{Li}_2(\mathbf{Z}_L), \end{aligned} \quad (3)$$

where $\text{Norm}(\cdot)$ is layer normalization. $\text{Li}(\cdot)$ means linear layer. Afterward, we aggregate global spatial information by projecting \mathbf{F}_R into query $\mathbf{Q} = \mathbf{W}_Q \mathbf{F}_R$ and key $\mathbf{K} = \mathbf{W}_K \mathbf{F}_L$ and transforming \mathbf{F}_L into value $\mathbf{V} = \mathbf{W}_V \mathbf{F}_L$, where \mathbf{W} is the combination of a 1×1 point-wise convolution and a 3×3 depth-wise convolution. We then perform cross-attention and get the output feature $\tilde{\mathbf{F}}$:

$$\tilde{\mathbf{F}} = \mathbf{F} + \text{SoftMax} \left(\mathbf{Q} \mathbf{K}^T / \sqrt{\tilde{C}} \right) \cdot \mathbf{V}, \quad (4)$$

where channels are split into multi-head for attention calculation. By doing so, RG-MCA introduces explicit guidance to fully exploit Retinex knowledge at the feature level and use cross attention mechanism to implicitly model the Retinex theory and refine the decomposed features, which helps to restore missing details and correct color distortion.

Then we employ DFA for local feature aggregation. Apart from the 1×1 convolution and 3×3 depth-wise convolution used for information aggregation, DFA also adopts GELU $\text{GELU}(\cdot)$ to ensure the flexibility of aggregation [18]. Thus, given $\tilde{\mathbf{F}}$, the output feature $\hat{\mathbf{F}}$ is

$$\begin{aligned} \hat{\mathbf{F}} &= \tilde{\mathbf{F}} + \text{GELU}(\mathbf{W}_1 \tilde{\mathbf{F}}) \odot \mathbf{W}_2 \tilde{\mathbf{F}}', \\ \tilde{\mathbf{F}}' &= \text{Li}_1(\mathbf{Z}) \odot \text{Norm}(\tilde{\mathbf{F}}) + \text{Li}_2(\mathbf{Z}), \end{aligned} \quad (5)$$

where $\mathbf{Z} = \text{conca}(\mathbf{Z}_R, \mathbf{Z}_L)$ and $\mathbf{Z} \in \mathbb{R}^{4C'}$.

Optimization. To facilitate the extraction of Retinex priors, the RPE module and RGformer are jointly trained by a reconstruction loss with L_1 norm $\|\cdot\|_1$:

$$L_{Rec} = \|\mathbf{I}_{GT} - \mathbf{I}_{HQ}\|_1, \quad (6)$$

where \mathbf{I}_{HQ} is the enhanced result. In addition, to ensure that the separated features within RG-MCA effectively capture reflectance and illumination knowledge, we provide an auxiliary decoder $D_a(\cdot)$ with the same structure as that in [35]. $D_a(\cdot)$ takes $\tilde{\mathbf{F}}$ as input and outputs the reconstructed reflectance image \mathbf{R}_{Re} and illumination map \mathbf{L}_{Re} . For efficiency, we only apply $D_a(\cdot)$ for the first transformer block in encoder to get \mathbf{R}_{Re}^I and \mathbf{L}_{Re}^I and for the last transformer block in decoder to get \mathbf{R}_{Re}^L and \mathbf{L}_{Re}^L . $D_a(\cdot)$ is supervised by a Retinex loss L_{Ret} , which is defined as

$$\begin{aligned} L_{Ret} &= \|\mathbf{R}_{LQ} - \mathbf{R}_{Re}^I\|_1 + \|\mathbf{L}_{LQ} - \mathbf{L}_{Re}^I\|_1 \\ &+ \|\mathbf{R}_{GT} - \mathbf{R}_{Re}^L\|_1 + \|\mathbf{L}_{GT} - \mathbf{L}_{Re}^L\|_1. \end{aligned} \quad (7)$$

The utilization of Eq. (7) serves a dual purpose: it not only facilitates the learning of Retinex theory by the split features but also enhances the overall restoration capacity.

In Phase I, the final loss L_{P1} is defined as:

$$L_{P1} = L_{Rec} + L_{Ret}. \quad (8)$$

3.2. Retinex-based Latent Diffusion Model

In Phase II, we train the Retinex-based latent diffusion model (RLDM) to predict Retinex priors. Different from conventional latent diffusion models that are typically trained on the RGB domain, we introduce two RLDMs with a Siamese structure and train them on distinct domains: the reflectance domain and the illumination domain, respectively. This approach, grounded in Retinex theory, equips our RLDM to generate a more generative reflectance prior denoted as $\hat{\mathbf{Z}}_R$ to enhance image details, and a more harmonized illumination prior $\hat{\mathbf{Z}}_L$ for color correction. To simplify, we provide a detailed derivation for $\hat{\mathbf{Z}}_R$ herein, while further elaboration on $\hat{\mathbf{Z}}_L$ can be found in the supplementary material (Supp). It's worth noting that RLDM is constructed upon the foundation of conditional denoising diffusion probabilistic models [5,55], comprising both a forward diffusion process and a reverse denoising process.

Diffusion process. In the diffusion process, we first use the pretrained RPE to extract the reflectance prior \mathbf{Z}_R , which is treated as the starting point of the forward Markov process, *i.e.*, $\mathbf{Z}_R = \mathbf{Z}_R^0$. We then gradually add Gaussian noise to \mathbf{Z}_R by T iterations and each iteration can be defined as:

$$q(\mathbf{Z}_R^t | \mathbf{Z}_R^{t-1}) = \mathcal{N} \left(\mathbf{Z}_R^t; \sqrt{1 - \beta^t} \mathbf{Z}_R^{t-1}, \beta^t \mathbf{I} \right), \quad (9)$$

where $t = 1, \dots, T$. \mathbf{Z}_R^t denotes the noisy prior at time step t , β^t is the predefined factor that controls the noise variance, and \mathcal{N} is the Gaussian distribution. Following [27], Eq. (9) can be simplified as follows:

$$q(\mathbf{Z}_R^t | \mathbf{Z}_R^0) = \mathcal{N} \left(\mathbf{Z}_R^t; \sqrt{\bar{\alpha}^t} \mathbf{Z}_R^0, (1 - \bar{\alpha}^t) \mathbf{I} \right), \quad (10)$$

Methods	Sources	LOL-v1				LOL-v2-real				LOL-v2-syn				SID			
		PSNR \uparrow	SSIM \uparrow	FID \downarrow	BIQE \downarrow	PSNR \uparrow	SSIM \uparrow	FID \downarrow	BIQE \downarrow	PSNR \uparrow	SSIM \uparrow	FID \downarrow	BIQE \downarrow	PSNR \uparrow	SSIM \uparrow	FID \downarrow	BIQE \downarrow
DeepLPF [44]	CVPR20	15.28	0.473	174.75	51.17	14.10	0.480	186.70	49.72	16.02	0.587	89.82	47.09	18.07	0.600	93.69	46.40
MIRNet [64]	ECCV20	24.14	0.835	71.16	47.75	20.02	0.820	82.25	41.18	21.94	0.876	40.18	36.29	20.84	0.605	81.37	40.63
EnGAN [24]	TIP21	17.48	0.656	153.98	35.82	18.23	0.617	173.28	51.06	16.57	0.734	93.66	45.59	17.23	0.543	77.52	33.47
DBRN [60]	TIP21	20.13	0.837	85.57	22.46	20.29	0.831	94.22	35.31	23.22	0.927	28.74	27.72	19.02	0.577	96.65	41.08
RUAS [33]	CVPR21	18.23	0.723	127.60	45.17	18.27	0.723	151.62	34.73	16.55	0.652	91.60	46.38	18.44	0.581	72.18	45.02
IPT [4]	CVPR21	16.27	0.504	158.83	29.35	19.80	0.813	97.24	31.17	18.30	0.811	76.79	42.15	20.53	0.618	70.58	36.71
URetinx [54]	CVPR22	21.33	0.835	85.59	30.37	20.44	0.806	76.74	28.85	24.73	0.897	33.25	33.46	22.09	0.633	71.58	38.44
UFormer [52]	CVPR22	16.36	0.771	166.69	41.06	18.82	0.771	164.41	40.36	19.66	0.871	58.69	39.75	18.54	0.577	100.14	42.13
Restormer [63]	CVPR22	22.43	0.823	78.75	33.18	19.94	0.827	114.35	37.27	21.41	0.830	46.89	35.06	22.27	0.649	75.47	32.49
SNR-Net [57]	CVPR22	24.61	0.842	66.47	28.73	21.48	0.849	68.56	28.83	24.14	0.928	30.52	33.47	22.87	0.625	74.78	30.08
SMG [58]	CVPR23	24.82	0.838	69.47	30.15	22.62	0.857	71.76	30.32	25.62	0.905	23.36	29.35	23.18	0.644	77.58	31.50
Retformer [2]	ICCV23	25.16	0.845	72.38	26.68	22.80	0.840	79.58	34.39	25.67	0.930	22.78	30.26	24.44	0.680	82.64	35.04
Diff-Retinx [62]	ICCV23	21.98	0.852	51.33	19.62	20.17	0.826	46.67	24.18	24.30	0.921	28.74	26.35	23.62	0.665	58.93	31.17
MRQ [34]	ICCV23	25.24	0.855	53.32	22.73	22.37	0.854	68.89	33.61	25.54	0.940	20.86	25.09	24.62	0.683	61.09	27.81
IAGC [51]	ICCV23	24.53	0.842	59.73	25.50	22.20	0.863	70.34	31.70	25.58	0.941	21.38	30.32	24.80	0.688	63.72	29.53
DiffIR [55]	ICCV23	23.15	0.828	70.13	26.38	21.15	0.816	72.33	29.15	24.76	0.921	28.87	27.74	23.17	0.640	78.80	30.56
CUE [68]	ICCV23	21.86	0.841	69.83	27.15	21.19	0.829	67.05	28.83	24.41	0.917	31.33	33.83	23.25	0.652	77.38	28.85
Reti-Diff (Ours)	—	25.35	0.866	49.14	17.75	22.97	0.858	43.18	23.66	27.53	0.951	13.26	15.77	25.53	0.692	51.66	25.58

Table 1. Results on low-light image enhancement. *LOL-v2-syn* denotes *LOL-v2-synthetic*. The best two results are in red and blue fonts.

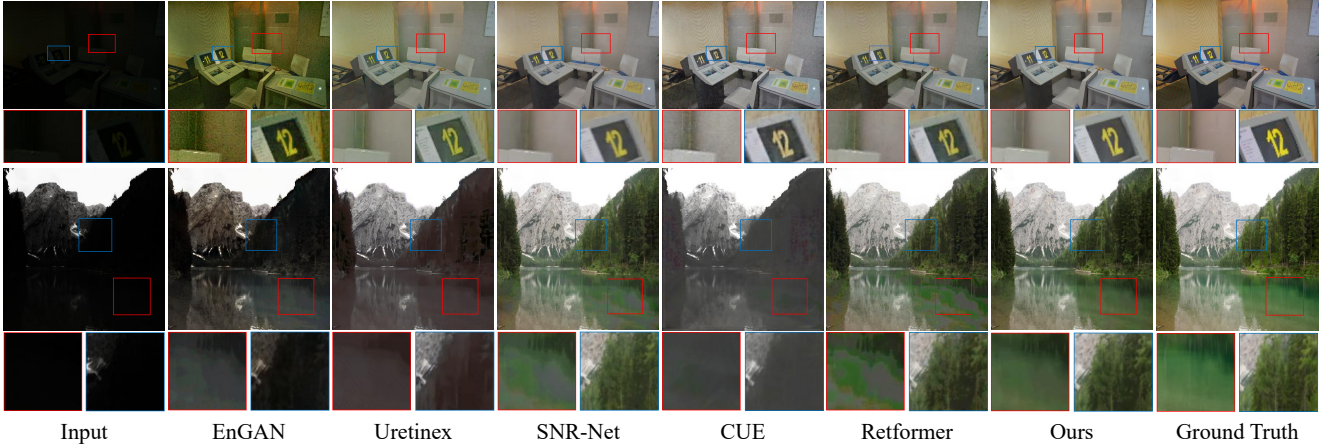


Figure 3. Visual results on the low-light image enhancement task.

where $\alpha^t = 1 - \beta^t$ and $\bar{\alpha}^t = \prod_{i=1}^t \alpha^i$.

Reverse process. In the reverse process, RLDM aims to extract the reflectance prior from pure Gaussian noise. Thus, RLDM samples a Gaussian random noise map \mathbf{Z}_R^T and then gradually denoise it to run backward from \mathbf{Z}_R^T to \mathbf{Z}_R^0 :

$$p(\mathbf{Z}_R^{t-1} | \mathbf{Z}_R^t, \mathbf{Z}_R^0) = \mathcal{N}(\mathbf{Z}_R^{t-1}; \boldsymbol{\mu}^t(\mathbf{Z}_R^t, \mathbf{Z}_R^0), (\boldsymbol{\sigma}^t)^2 \mathbf{I}), \quad (11)$$

where mean $\boldsymbol{\mu}^t(\mathbf{Z}_R^t, \mathbf{Z}_R^0) = \frac{1}{\sqrt{\alpha^t}}(\mathbf{Z}_R^t - \frac{1-\alpha^t}{\sqrt{1-\bar{\alpha}^t}}\boldsymbol{\epsilon})$ and variance $(\boldsymbol{\sigma}^t)^2 = \frac{1-\bar{\alpha}^{t-1}}{1-\bar{\alpha}^t}\beta^t$. $\boldsymbol{\epsilon}$ denotes the noise in \mathbf{Z}_R^t and is the only uncertain variable. Following previous practice [55], we employ a denoising network $\epsilon_\theta(\cdot)$ to estimate $\boldsymbol{\theta}$. To operate in the latent space, we further introduce another RPE module $\widetilde{\text{RPE}}(\cdot)$ to extract the conditional reflectance vector $\mathbf{V}_R \in \mathbb{R}^{3C'}$ from the reflectance image \mathbf{R}_{LQ} of the LQ image, i.e., $\mathbf{V}_R = \widetilde{\text{RPE}}(\text{down}(\mathbf{R}_{LQ}))$. Therefore, the denoising network can be represented by $\epsilon_\theta(\mathbf{Z}_R^t, \mathbf{V}_R, t)$. By setting the variance to $1 - \alpha^t$, we get

$$\mathbf{Z}_R^{t-1} = \frac{1}{\sqrt{\alpha^t}}(\mathbf{Z}_R^t - \frac{1-\alpha^t}{\sqrt{1-\bar{\alpha}^t}}\epsilon_\theta(\mathbf{Z}_R^t, \mathbf{V}_R, t)) + \sqrt{1-\alpha^t}\boldsymbol{\epsilon}^t, \quad (12)$$

where $\boldsymbol{\epsilon}^t \sim \mathcal{N}(0, \mathbf{I})$. By using Eq. (12) for T iterations, we

can get the predicted prior $\hat{\mathbf{Z}}_R$ and use it to guide RGformer for image restoration. Because the size of the predicted prior $\hat{\mathbf{Z}}_R \in \mathbb{R}^{3C'}$ is much smaller than the original reflectance image $\mathbf{R}_{LQ} \in \mathbb{R}^{H \times W \times C}$, RLDM needs much less iterations than those image-level diffusion models [62]. Thus, we run the complete T iterations for the prior generation rather than randomly selecting one time step.

Optimization. Having got the predicted priors $\hat{\mathbf{Z}}_R$ and $\hat{\mathbf{Z}}_L$, which are generated by two Siamese RLDMs with specific weights, we propose the diffusion loss to supervise them:

$$L_{Dif} = \|\mathbf{Z}_R - \hat{\mathbf{Z}}_R\|_1 + \|\mathbf{Z}_L - \hat{\mathbf{Z}}_L\|_1. \quad (13)$$

For restoration quality, we propose joint training RPE, RGformer, and RLDM. Thus, the loss in Phase II is

$$L_{P2} = L_{Dif} + L_{Rec} + L_{Ret}. \quad (14)$$

3.3. Inference

In the inference phase, given the LQ input \mathbf{I}_{LQ} , Reti-Diff first uses RPE to extract the conditional vectors \mathbf{V}_R and \mathbf{V}_L , and then generates predicted Retinex priors $\hat{\mathbf{Z}}_R$ and $\hat{\mathbf{Z}}_L$ with two RLDMs. Under the guidance of the Retinex

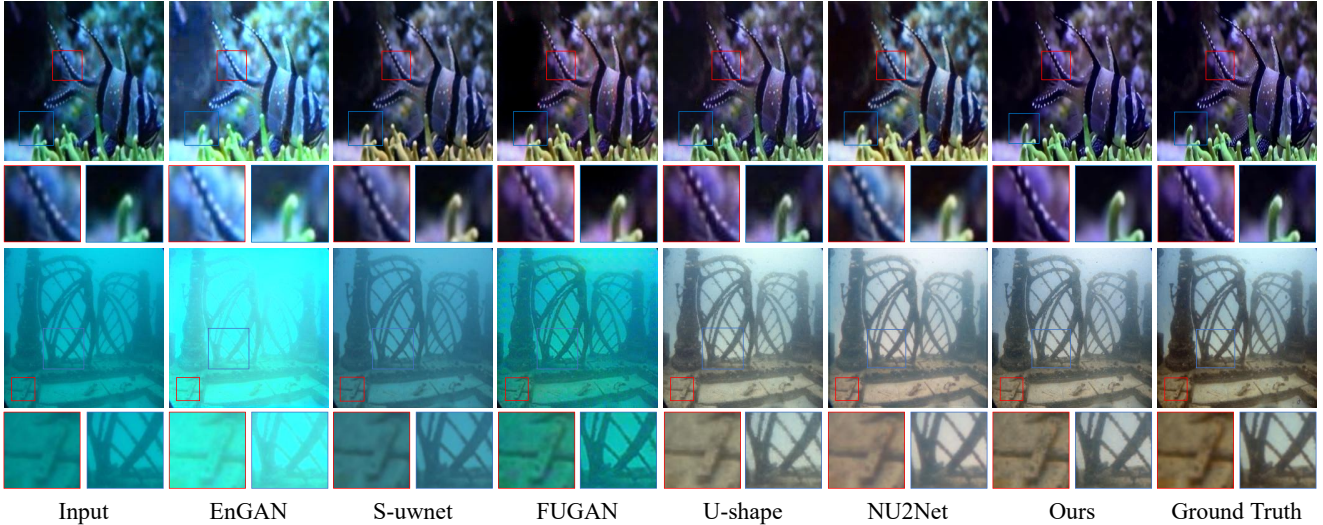


Figure 4. Visual results on the underwater image enhancement task.

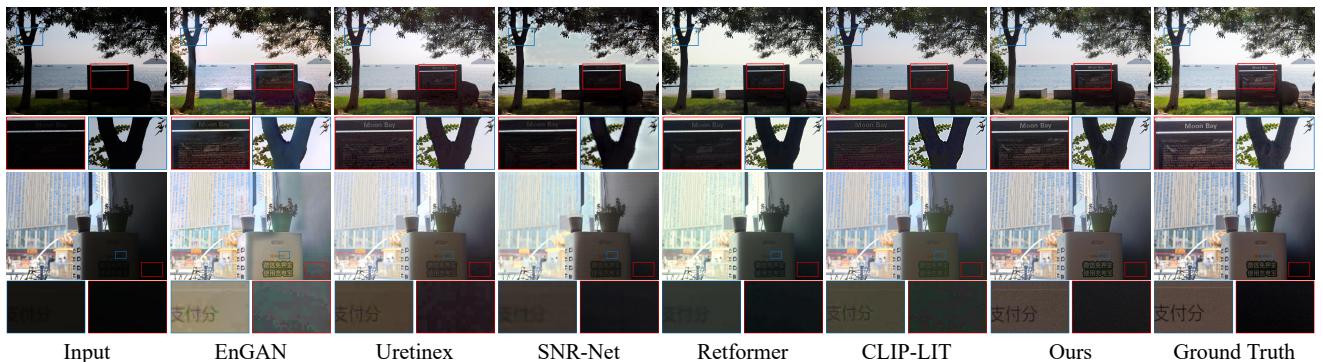


Figure 5. Visual results on the backlit image enhancement task.

priors, RGformer generates the restored HQ image I_{HQ} . Benefiting from our Retinex-based framework, I_{HQ} enjoys richer texture details and more harmonized illumination.

4. Experiment

4.1. Experimental Setup

Our Reti-Diff is implemented in PyTorch on four RTX3090TI GPUs and is optimized by Adam with momentum terms (0.9, 0.999). In phases I and II, we train the network for 300K iterations and the learning rate is initially set as 2×10^{-4} and gradually reduced to 1×10^{-6} with the cosine annealing [38]. Following [2, 62], random rotation and flips are used for augmentation. Reti-Diff mainly comprises RLDM and RGformer. For RLDM, the channel number C' is set as 64. The total time step T is set to 4 and the hyperparameters $\beta^{1:T}$ linearly increase from $\beta^1 = 0.1$ to $\beta^T = 0.99$. RGformer adopts a 4-level cascade encoder-decoder structure. We set the number of transformer blocks, the attention heads, and the channel number as [3, 3, 3, 3], [1, 2, 4, 8], and [64, 128, 256, 512] from level 1 to level 4.

4.2. Comparative Evaluation

Low-light Image Enhancement. We conduct a comprehensive evaluation on four datasets: *LOL-v1* [53], *LOL-v2-real* [61], *LOL-v2-syn* [61], and *SID* [3]. We adhere to the training manner outlined in [2]. Our assessment involves four metrics: PSNR, SSIM, FID [21], and BIQE [43]. Note that larger PSNR and SSIM scores, as well as smaller FID and BIQE scores, denote superior performance. We compare our approach against 17 cutting-edge enhancement techniques and report the results in Tab. 1. As depicted in Tab. 1, our method emerges as the top performer across all datasets and significantly outperforms the second-best method (Diff-Retinex) by 13.2%. These results underscore the superiority of our Reti-Diff. Fig. 3 presents qualitative results, showcasing our capacity to generate enhanced images with corrected illumination and enhanced texture, even in extremely challenging conditions. In contrast, existing methods struggle to achieve the same level of performance such as the boundaries of power lines, color harmonization of lakes, and detailed textures of wooded areas. Notably, results from the compared methods are generated with their provided models under the same settings to ensure fairness.

Methods	Sources	UIEB				LSUI			
		PSNR \uparrow	SSIM \uparrow	UCIQE \uparrow	UIQM \uparrow	PSNR \uparrow	SSIM \uparrow	UCIQE \uparrow	UIQM \uparrow
FUGAN [23]	IRAL20	17.41	0.842	0.527	2.614	22.16	0.837	0.576	2.667
EnGAN [24]	TIP21	17.73	0.833	0.529	2.465	19.30	0.851	0.587	2.817
Ucolor [29]	TIP21	20.78	0.868	0.537	3.049	22.91	0.886	0.594	2.735
S-uwnet [45]	AAAI21	18.28	0.855	0.544	2.942	20.89	0.875	0.582	2.746
PUIE [14]	ECCV22	21.38	0.882	0.566	3.021	23.70	0.902	0.605	2.974
U-shape [47]	TIP23	22.91	0.905	0.592	2.896	24.16	0.917	0.603	3.022
PUGAN [7]	TIP23	23.05	0.897	0.608	2.902	25.06	0.916	0.629	3.106
ADP [69]	IJCV23	22.90	0.892	0.621	3.005	24.28	0.913	0.626	3.075
NU2Net [15]	AAAI23	22.38	0.903	0.587	2.936	25.07	0.908	0.615	3.112
Reti-Diff (Ours)	—	24.12	0.910	0.631	3.088	28.10	0.929	0.646	3.208

Table 2. Results on underwater image enhancement.

Metrics	RLDM		RGformer			Train	-
	w/o RLDM	w/o Retinex	w/o DFA	w/o RG-MCA	w/o $D_a(\cdot)$	w/o joint	Ours
PSNR	25.38	26.25	26.49	25.92	26.80	27.18	27.53
SSIM	0.918	0.939	0.925	0.913	0.944	0.947	0.951

Table 4. Ablation study on the low-light image enhancement task.

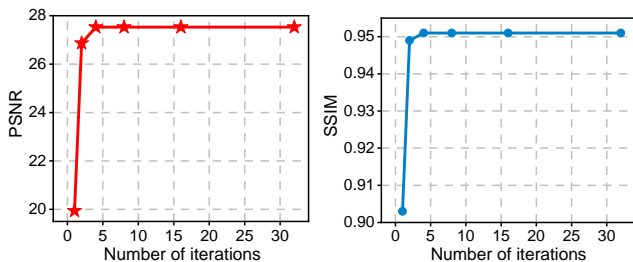


Figure 6. Ablation study of the number of iterations in RLDM.

Underwater Image Enhancement. We extend our evaluation to encompass two widely-used underwater image enhancement datasets: *UIEB* [30] and *LSUI* [47]. In addition to PSNR and SSIM, we employ two metrics specifically tailored for underwater images, namely UCIQE [59] and UIQM [46], to assess the performance of the ten enhancement approaches. In all cases, higher values indicate superior performance. The results are presented in Tab. 2. As showcased in Tab. 2, our method achieved the highest overall performance and outperformed the second-best method (PUGAN) by 4.48%. A qualitative analysis is presented in Fig. 4, illustrating our method’s ability to correct underwater color aberrations and highlight fine texture details.

Backlit Image Enhancement. Following CLIP-LIT [32], we select the *BAID* [40] dataset for training the network with an image size of 256×256 . In addition to PSNR and SSIM, our evaluation incorporates LPIPS [66] and FID [21] as metrics for evaluation. In this case, lower LPIPS scores and FID scores denote superior performance. The evaluation results are reported in Tab. 3. As demonstrated in Tab. 3, our method excels in all metrics and generally outperformed the second-best method (CLIP-LIT) by 6.03%. Furthermore, a visual comparison in Fig. 5 provides additional evidence of our superiority in detail reconstruction and color correction. All methods are trained by cropping the training data as 256×256 for fairness.

Methods	Sources	BAID			
		PSNR \uparrow	SSIM \uparrow	LPIPS \downarrow	FID \downarrow
EnGAN [24]	TIP21	17.96	0.819	0.182	43.55
RUAS [33]	CVPR21	18.92	0.813	0.262	40.07
URetinex [54]	CVPR22	19.08	0.845	0.206	42.26
SNR-Net [57]	CVPR22	20.86	0.860	0.213	39.73
Restormer [63]	CVPR22	21.07	0.832	0.192	41.17
Retformer [2]	ICCV23	22.03	0.862	0.173	45.27
CLIP-LIT [32]	ICCV23	21.13	0.853	0.159	37.30
Diff-Retinex [62]	ICCV23	22.07	0.861	0.160	38.07
DiffIR [55]	ICCV23	21.10	0.835	0.175	40.35
Reti-Diff (Ours)	—	23.19	0.876	0.147	27.47

Table 3. Results on backlit image enhancement.

Metrics	Res [63]	Res+RLDM	Ret [2]	Ret+RLDM
	PSNR	21.41	24.15	25.67
SSIM	0.830	0.862	0.930	0.942
Gain	—	8.33%	—	2.87%

Table 5. Generalization of RLDM.

4.3. Ablation Study

We conduct ablation studies on the low-light image enhancement task with the *LOL-v2-syn* dataset.

Effect of RLDM. As illustrated in Tab. 4, we ablate RLDM by directly removing RLDM or retraining RLDM in the RGB domain, *i.e.*, w/o Retinex, rather than in the reflectance and illumination domain (RGformer is guided by one RGB prior instead of the Retinex priors in this time). The two modifications result in significant drops in performance. This outcome underscores the critical role of RLDM in enhancing the restoration process. Furthermore, to assess the generalizability of RLDM, we conducted additional experiments by replacing our RGformer with two transformer-based frameworks, namely Res (Restormer [63]) and Ret (Retformer [2]). Note that the training settings are kept consistent with our Reti-Diff. The results are presented in Tab. 5. Tab. 5 reveals that RLDM significantly improves the performance of both frameworks, where “Gain” is the average gain of PSNR and SSIM. This demonstrates that our RLDM serves as a plug-and-play module with strong generalization capabilities.

Effect of RGformer. We conduct an analysis to assess the impact of our RGformer, and the results are presented in Tab. 4. In this study, we systematically removed critical components, such as DFA, RG-MCA, and the auxiliary decoder $D_a(\cdot)$, from the model architecture. The outcomes of this ablation study clearly indicate that the performance deteriorates when these components are removed, highlighting their essential role in the system. Additionally, in Tab. 4, we conduct an evaluation to affirm the significance of joint training in our approach. This analysis reinforces the importance of the joint training process.

Ablations on iteration number. The number of iterations in the diffusion model plays a crucial role in determining the method’s efficiency. To explore this, we conducted experiments with different iteration numbers for Reti-Diff, specif-

Methods	<i>L-v1</i>	<i>L-v2-R</i>	<i>L-v2-S</i>	<i>SID</i>	Mean
EnGAN [24]	2.63	1.69	2.23	1.24	1.95
RUAS [33]	3.57	3.06	3.01	2.23	2.97
Restormer [63]	3.26	3.32	3.41	2.53	3.13
Uretinex [54]	3.82	3.98	3.70	3.28	3.70
SNR-Net [57]	3.76	4.12	3.58	3.42	3.72
CUE [68]	3.62	3.81	3.28	3.09	3.45
Retformer [2]	3.35	4.02	3.71	3.35	3.61
Ours	4.05	4.33	3.92	3.75	4.01

Table 6. User study in low-light enhancement.

Methods (AP)	Bicycle	Boat	Bottle	Bus	Car	Cat	Chair	Cup	Dog	Motor	People	Table	Mean
RetinexNet [53]	73.8	62.8	64.8	84.9	80.8	53.4	57.2	68.3	61.5	51.3	65.9	43.1	64.0
KinD [67]	72.2	66.5	58.9	83.7	74.5	55.4	61.7	61.3	63.8	63.0	70.5	47.8	65.0
MIRNet [64]	71.8	63.8	62.9	81.4	71.1	58.8	58.9	61.3	63.1	52.0	68.8	45.5	63.6
RUAS [33]	72.0	62.2	65.2	72.9	78.1	57.3	62.4	61.8	60.2	61.5	69.4	46.8	64.2
Restormer [63]	76.2	65.1	64.2	84.0	76.3	59.2	53.0	58.7	66.1	62.9	68.6	45.0	64.9
SNR-Net [57]	75.3	64.4	63.6	85.3	77.5	59.1	54.1	59.6	66.3	65.2	69.1	44.6	65.3
SCI [42]	74.6	65.3	65.8	85.4	76.3	59.4	57.1	60.5	65.6	63.9	69.1	45.9	65.6
Retformer [2]	76.3	66.7	65.9	84.7	77.6	61.2	53.5	60.7	67.5	63.4	69.5	46.0	66.1
Ours	83.0	78.1	77.2	91.8	85.5	72.4	68.4	79.4	81.0	81.6	82.7	57.2	78.2

Table 7. Low-light image detection on *ExDark* [36].

Methods (IoU)	Bicycle	Boat	Bottle	Bus	Car	Cat	Chair	Dog	Horse	People	Mean
RetinexNet [53]	45.32	29.63	50.07	76.62	66.83	52.36	17.75	43.06	59.45	57.73	49.88
KinD [67]	50.06	31.75	51.18	70.19	69.08	50.75	13.33	45.71	58.81	58.82	49.97
MIRNet [64]	51.16	37.79	45.52	70.07	65.10	52.26	18.84	47.05	60.06	55.19	50.30
RUAS [33]	52.08	35.59	47.95	68.26	73.35	48.73	20.09	47.73	61.18	56.68	51.16
Restormer [63]	51.19	34.86	52.16	60.19	67.23	50.72	21.17	50.64	63.78	58.64	51.06
SNR-Net [57]	52.24	36.28	50.17	75.58	72.26	51.66	22.74	52.26	61.42	59.35	53.40
SCI [42]	48.83	43.38	51.03	73.35	70.08	43.11	18.82	49.92	60.85	62.58	52.20
Retformer [2]	40.07	38.82	47.74	69.92	63.78	54.19	14.53	48.35	61.07	61.72	50.02
Ours	59.75	51.47	62.06	85.52	76.58	57.72	28.86	56.31	66.20	73.35	61.78

Table 8. Low-light semantic segmentation, where images are darkened by [65].

Methods	<i>COD10K</i>				<i>NC4K</i>			
	$M \downarrow$	$F_\beta \uparrow$	$E_\phi \uparrow$	$S_\alpha \uparrow$	$M \downarrow$	$F_\beta \uparrow$	$E_\phi \uparrow$	$S_\alpha \uparrow$
RetinexNet [53]	0.041	0.667	0.845	0.789	0.055	0.750	0.842	0.819
KinD [67]	0.039	0.673	0.849	0.792	0.052	0.762	0.875	0.822
MIRNet [64]	0.037	0.697	0.857	0.799	0.049	0.802	0.888	0.833
RUAS [33]	0.036	0.705	0.861	0.803	0.051	0.795	0.883	0.827
Restormer [63]	0.036	0.700	0.859	0.800	0.050	0.792	0.880	0.830
SNR-Net [57]	0.036	0.703	0.865	0.803	0.049	0.801	0.892	0.838
SCI [42]	0.037	0.710	0.863	0.805	0.051	0.782	0.880	0.836
Retformer [2]	0.037	0.682	0.861	0.806	0.052	0.766	0.881	0.832
Ours	0.034	0.725	0.880	0.813	0.047	0.804	0.897	0.841

Table 9. Low-light concealed object segmentation.

ically T values selected from the set $\{1, 2, 4, 8, 16, 32\}$. We adjusted the β^t parameter as defined in Eq. (9) accordingly. The results in terms of PSNR for different iterations, as shown in Fig. 6, illustrate that Reti-Diff exhibits rapid convergence and generates stable guidance priors with just 4 iterations. This efficiency is attributed to our application of the diffusion model within the compact latent space.

4.4. User Study and Downstream Tasks

User Study. We conduct a user study to assess the subjective visual perception of low-light image enhancement. In this study, 29 human subjects are invited to assign scores to the enhanced results based on four criteria: (1) The presence of underexposed or overexposed regions. (2) The existence of color distortion. (3) The occurrence of undesired noise or artifacts. (4) The inclusion of essential structural details. Participants rate the results on a scale from 1 (worst) to 5 (best). Each low-light image is presented alongside its enhanced results, with the names of the enhancement methods concealed from the evaluators. The scores are reported in Tab. 6. As shown in Tab. 6, our method receives the highest scores across all four datasets, which highlights our effectiveness in generating visually appealing results.

Low-light Object Detection. The enhanced images are expected to have better downstream performance than the original ones. We first verify this on low-light object detection. Following [2], all the compared methods are performed on *ExDark* [36] with YOLOv3, which is trained from scratch. As shown in Tab. 7, our Reti-Diff exhibits a substantial advantage over existing methods, as evidenced by higher average precision (AP) scores. Notably, the mean AP of our method surpasses that of the second-best performing method, Retformer [2], by an impressive margin

of 12.1 AP points, which serves as compelling evidence of our efficacy in facilitating high-level vision understanding.

Low-light Image Segmentation. We extend our experimentation to include image segmentation tasks, specifically semantic segmentation and concealed object segmentation. For semantic segmentation, following [25], we apply image darkening to samples from the *VOC* [9] dataset according to [65]. We then employ Mask2Former [6], a state-of-the-art segmentor, to perform segmentation on the enhanced results of these darkened images. The evaluation metric used is Intersection over Union (IoU), and the results are presented in Tab. 8. As shown in Tab. 8, our method achieves the highest performance across all classes, surpassing the second-best method by a substantial margin of 15.7%.

We further venture into concealed object segmentation (COS) on *COD10K* [10] and *NC4K* [41], which represent a challenging segmentation task aimed at delineating objects with inherent background similarity. We also apply image darkening [65] and enlist the cutting-edge COS segmentor, FEDER [18], to perform segmentation on the enhanced results. We evaluate the results using four metrics: mean absolute error (M), adaptive F-measure (F_β), mean E-measure (E_ϕ), and structure measure (S_α), which are presented in Tab. 9. As depicted in Tab. 9, our method exhibits superior performance compared to the second-best method, SNR-Net, with a notable margin of 2.1% on average. Collectively, the exceptional results achieved in these two segmentation tasks substantiate our proficiency in recovering image-level illumination degraded information.

5. Future Works

In future work, we consider the use of multimodal data [11] to aid in improving image reconstruction perfor-

mance, such as using infrared images [17, 56] to aid in low-light visible image enhancement. Besides, We will explore whether our approach is downstream task-friendly with more segmentation algorithms [19, 48].

6. Conclusions

To mitigate pixel misalignment, our approach adopt DM within a compact latent space to generate guidance priors. Specifically, we introduce RLDM to extract Retinex priors, which are subsequently supplied to RGformer for feature decomposition. This process ensures precise detailed reconstruction and effective illumination correction. RGformer then refines and aggregates the decomposed features, enhancing the robustness in handling complex degradation scenarios. Our approach is extensively validated through experiments, establishing the clear superiority of Reti-Diff.

References

- [1] Mohammad Abdullah-Al-Wadud, Md Hasanul Kabir, M Ali Akber Dewan, and Oksam Chae. A dynamic histogram equalization for image contrast enhancement. *IEEE transactions on consumer electronics*, 53(2):593–600, 2007. [2](#)
- [2] Yuanhao Cai, Hao Bian, Jing Lin, Haoqian Wang, Radu Timofte, and Yulun Zhang. Retinexformer: One-stage retinex-based transformer for low-light image enhancement. In *ICCV*, pages 12504–12513, 2023. [1](#), [2](#), [4](#), [5](#), [6](#), [7](#), [8](#)
- [3] Chen Chen, Qifeng Chen, Minh N Do, and Vladlen Koltun. Seeing motion in the dark. In *ICCV*, pages 3185–3194, 2019. [6](#)
- [4] Hanting Chen, Yunhe Wang, Tianyu Guo, Chang Xu, Yiping Deng, Zhenhua Liu, Siwei Ma, Chunjing Xu, Chao Xu, and Wen Gao. Pre-trained image processing transformer. In *CVPR*, pages 12299–12310, 2021. [5](#)
- [5] Zheng Chen, Yulun Zhang, Ding Liu, Bin Xia, Jinjin Gu, Linghe Kong, and Xin Yuan. Hierarchical integration diffusion model for realistic image deblurring. In *NeurIPS*, 2023. [2](#), [3](#), [4](#)
- [6] Bowen Cheng, Ishan Misra, Alexander G Schwing, Alexander Kirillov, and Rohit Girdhar. Masked-attention mask transformer for universal image segmentation. In *Proceedings of the IEEE/CVF conference on computer vision and pattern recognition*, pages 1290–1299, 2022. [8](#)
- [7] Runmin Cong, Wenyu Yang, Wei Zhang, Chongyi Li, Chunle Guo, Qingming Huang, and Sam Kwong. Pagan: Physical model-guided underwater image enhancement using gan with dual-discriminators. *IEEE Transactions on Image Processing*, 2023. [1](#), [7](#)
- [8] Lizhen Deng, Chunming He, Guoxia Xu, Hu Zhu, and Hao Wang. Pegan: A noise robust conditional generative adversarial network for one shot learning. *IEEE Transactions on Intelligent Transportation Systems*, 23(12):25249–25258, 2022. [2](#)
- [9] Mark Everingham, Luc Van Gool, Christopher KI Williams, John Winn, and Andrew Zisserman. The pascal visual object classes (voc) challenge. *International journal of computer vision*, 88:303–338, 2010. [8](#)
- [10] Deng-Ping Fan, Ge-Peng Ji, Ming-Ming Cheng, and Ling Shao. Concealed object detection. *IEEE transactions on pattern analysis and machine intelligence*, 44(10):6024–6042, 2021. [8](#)
- [11] Cheng-Yu Fang and Xian-Feng Han. Joint geometric-semantic driven character line drawing generation. In *ICMR*, pages 226–233, 2023. [8](#)
- [12] Xueyang Fu, Delu Zeng, Yue Huang, Yinghao Liao, Xinghao Ding, and John Paisley. A fusion-based enhancing method for weakly illuminated images. *Signal Processing*, 129:82–96, 2016. [1](#)
- [13] Xueyang Fu, Delu Zeng, Yue Huang, Xiao-Ping Zhang, and Xinghao Ding. A weighted variational model for simultaneous reflectance and illumination estimation. In *CVPR*, pages 2782–2790, 2016. [2](#)
- [14] Zhenqi Fu, Wu Wang, Yue Huang, Xinghao Ding, and Kai-Kuang Ma. Uncertainty inspired underwater image enhancement. In *ECCV*, pages 465–482. Springer, 2022. [7](#)
- [15] Chunle Guo, Ruiqi Wu, Xin Jin, Linghao Han, Weidong Zhang, Zhi Chai, and Chongyi Li. Underwater ranker: Learn which is better and how to be better. In *AAAI*, volume 37, pages 702–709, 2023. [1](#), [7](#)
- [16] Chunming He, Kai Li, Guoxia Xu, Jiangpeng Yan, Longxiang Tang, Yulun Zhang, Yaowei Wang, and Xiu Li. Hqg-net: Unpaired medical image enhancement with high-quality guidance. *IEEE Transactions on Neural Networks and Learning Systems*, 2023. [2](#)
- [17] Chunming He, Kai Li, Guoxia Xu, Yulun Zhang, Runze Hu, Zhenhua Guo, and Xiu Li. Degradation-resistant unfolding network for heterogeneous image fusion. In *ICCV*, pages 12611–12621, 2023. [9](#)
- [18] Chunming He, Kai Li, Yachao Zhang, Longxiang Tang, Yulun Zhang, Zhenhua Guo, and Xiu Li. Camouflaged object detection with feature decomposition and edge reconstruction. In *CVPR*, pages 22046–22055, 2023. [4](#), [8](#)
- [19] Chunming He, Kai Li, Yachao Zhang, Guoxia Xu, Longxiang Tang, Yulun Zhang, Zhenhua Guo, and Xiu Li. Weakly-supervised concealed object segmentation with sam-based pseudo labeling and multi-scale feature grouping. *arXiv preprint arXiv:2305.11003*, 2023. [9](#)
- [20] Chunming He, Kai Li, Yachao Zhang, Yulun Zhang, Zhenhua Guo, Xiu Li, Martin Danelljan, and Fisher Yu. Strategic preys make acute predators: Enhancing camouflaged object detectors by generating camouflaged objects. *arXiv preprint arXiv:2308.03166*, 2023. [2](#)
- [21] Martin Heusel, Hubert Ramsauer, Thomas Unterthiner, Bernhard Nessler, and Sepp Hochreiter. Gans trained by a two time-scale update rule converge to a local nash equilibrium. *NeurIPS*, 30, 2017. [6](#), [7](#)
- [22] Shih-Chia Huang, Fan-Chieh Cheng, and Yi-Sheng Chiu. Efficient contrast enhancement using adaptive gamma correction with weighting distribution. *IEEE transactions on image processing*, 22(3):1032–1041, 2012. [2](#)
- [23] Md Jahidul Islam, Youya Xia, and Junaed Sattar. Fast underwater image enhancement for improved visual perception. *IEEE Robotics and Automation Letters*, 5(2):3227–3234, 2020. [7](#)
- [24] Yifan Jiang, Xinyu Gong, Ding Liu, Yu Cheng, Chen Fang, Xiaohui Shen, Jianchao Yang, Pan Zhou, and Zhangyang Wang. Enlightengan: Deep light enhancement without paired supervision. *IEEE transactions on image processing*, 30:2340–2349, 2021. [1](#), [2](#), [5](#), [7](#), [8](#)
- [25] Mingye Ju, Charles A Guo, Chuheng Chen, Jinshan Pan, Jinhui Tang, and Dacheng Tao. Sllen: Semantic-aware low-light image enhancement network. *arXiv preprint arXiv:2211.11571*, 2022. [8](#)
- [26] Diederik Kingma, Tim Salimans, Ben Poole, and Jonathan Ho. Variational diffusion models. *NeurIPS*, 34:21696–21707, 2021. [2](#)
- [27] Diederik P Kingma and Max Welling. Auto-encoding variational bayes. *arXiv preprint arXiv:1312.6114*, 2013. [4](#)
- [28] Edwin H Land. The retinex theory of color vision. *Scientific american*, 237(6):108–129, 1977. [2](#)

- [29] Chongyi Li, Saeed Anwar, Junhui Hou, Runmin Cong, Chunle Guo, and Wenqi Ren. Underwater image enhancement via medium transmission-guided multi-color space embedding. *IEEE Transactions on Image Processing*, 30:4985–5000, 2021. 7
- [30] Chongyi Li, Chunle Guo, Wenqi Ren, Runmin Cong, Junhui Hou, Sam Kwong, and Dacheng Tao. An underwater image enhancement benchmark dataset and beyond. *IEEE Transactions on Image Processing*, 29:4376–4389, 2019. 7
- [31] Mading Li, Jiaying Liu, Wenhan Yang, Xiaoyan Sun, and Zongming Guo. Structure-revealing low-light image enhancement via robust retinex model. *IEEE Transactions on Image Processing*, 27(6):2828–2841, 2018. 2
- [32] Zhixin Liang, Chongyi Li, Shangchen Zhou, Ruicheng Feng, and Chen Change Loy. Iterative prompt learning for unsupervised backlit image enhancement. In *ICCV*, pages 8094–8103, 2023. 1, 7
- [33] Risheng Liu, Long Ma, Jiaao Zhang, Xin Fan, and Zhongxuan Luo. Retinex-inspired unrolling with cooperative prior architecture search for low-light image enhancement. In *CVPR*, pages 10561–10570, 2021. 1, 5, 7, 8
- [34] Yunlong Liu, Tao Huang, Weisheng Dong, Fangfang Wu, Xin Li, and Guangming Shi. Low-light image enhancement with multi-stage residue quantization and brightness-aware attention. In *ICCV*, pages 12140–12149, 2023. 5
- [35] Francesco Locatello, Dirk Weissenborn, Thomas Unterthiner, Aravindh Mahendran, Georg Heigold, Jakob Uszkoreit, Alexey Dosovitskiy, and Thomas Kipf. Object-centric learning with slot attention. *NeurIPS*, 33:11525–11538, 2020. 4
- [36] Yuen Peng Loh and Chee Seng Chan. Getting to know low-light images with the exclusively dark dataset. *Computer Vision and Image Understanding*, 178:30–42, 2019. 1, 8
- [37] Kin Gwn Lore, Adedotun Akintayo, and Soumik Sarkar. Llnet: A deep autoencoder approach to natural low-light image enhancement. *Pattern Recognition*, 61:650–662, 2017. 2
- [38] I Loshchilov and F Hutter. Stochastic gradient descent with warm restarts. In *ICLR*, pages 1–16, 2016. 6
- [39] Andreas Lugmayr, Martin Danelljan, Andres Romero, Fisher Yu, Radu Timofte, and Luc Van Gool. Repaint: Inpainting using denoising diffusion probabilistic models. In *CVPR*, pages 11461–11471, 2022. 3
- [40] Xiaoqian Lv, Shengping Zhang, Qinglin Liu, Haozhe Xie, Bineng Zhong, and Huiyu Zhou. Backlitnet: A dataset and network for backlit image enhancement. *Computer Vision and Image Understanding*, 218:103403, 2022. 1, 7
- [41] Yunqiu Lv, Jing Zhang, Yuchao Dai, Aixuan Li, Bowen Liu, Nick Barnes, and Deng-Ping Fan. Simultaneously localize, segment and rank the camouflaged objects. In *CVPR*, pages 11591–11601, 2021. 8
- [42] Long Ma, Tengyu Ma, Risheng Liu, Xin Fan, and Zhongxuan Luo. Toward fast, flexible, and robust low-light image enhancement. In *CVPR*, pages 5637–5646, 2022. 1, 8
- [43] Anush Krishna Moorthy and Alan Conrad Bovik. A two-step framework for constructing blind image quality indices. *IEEE Signal processing letters*, 17(5):513–516, 2010. 6
- [44] Sean Moran, Pierre Marza, Steven McDonagh, Sarah Parisot, and Gregory Slabaugh. Deeplpf: Deep local parametric filters for image enhancement. In *CVPR*, pages 12826–12835, 2020. 5
- [45] Ankita Naik, Apurva Swarnakar, and Kartik Mittal. Shallow-wnet: Compressed model for underwater image enhancement (student abstract). In *AAAI*, volume 35, pages 15853–15854, 2021. 7
- [46] Karen Panetta, Chen Gao, and Sos Agaian. Human-visual-system-inspired underwater image quality measures. *IEEE Journal of Oceanic Engineering*, 41(3):541–551, 2015. 7
- [47] Lintao Peng, Chunli Zhu, and Liheng Bian. U-shape transformer for underwater image enhancement. *IEEE Transactions on Image Processing*, 2023. 1, 7
- [48] Longxiang Tang, Kai Li, Chunming He, Yulun Zhang, and Xiu Li. Source-free domain adaptive fundus image segmentation with class-balanced mean teacher. In *MICCAI*, pages 684–694. Springer, 2023. 9
- [49] Neng-Tsann Ueng and Louis L Scharf. The gamma transform: A local time-frequency analysis method. In *ACSSC*, volume 2, pages 920–924. IEEE, 1995. 1
- [50] Ruixing Wang, Qing Zhang, Chi-Wing Fu, Xiaoyong Shen, Wei-Shi Zheng, and Jiaya Jia. Underexposed photo enhancement using deep illumination estimation. In *CVPR*, pages 6849–6857, 2019. 2
- [51] Yinglong Wang, Zhen Liu, Jianzhuang Liu, Songcen Xu, and Shuaicheng Liu. Low-light image enhancement with illumination-aware gamma correction and complete image modelling network. In *ICCV*, pages 13128–13137, 2023. 5
- [52] Zhendong Wang, Xiaodong Cun, Jianmin Bao, Wengang Zhou, Jianzhuang Liu, and Houqiang Li. Uformer: A general u-shaped transformer for image restoration. In *CVPR*, pages 17683–17693, 2022. 5
- [53] Chen Wei, Wenjing Wang, Wenhan Yang, and Jiaying Liu. Deep retinex decomposition for low-light enhancement. *arXiv preprint arXiv:1808.04560*, 2018. 6, 8
- [54] Wenhui Wu, Jian Weng, Pingping Zhang, Xu Wang, Wenhan Yang, and Jianmin Jiang. Uretinex-net: Retinex-based deep unfolding network for low-light image enhancement. In *CVPR*, pages 5901–5910, 2022. 5, 7, 8
- [55] Bin Xia, Yulun Zhang, Shiyin Wang, Yitong Wang, Xinglong Wu, Yapeng Tian, Wenming Yang, and Luc Van Gool. Diffir: Efficient diffusion model for image restoration. In *ICCV*, 2023. 1, 2, 3, 4, 5, 7
- [56] Guoxia Xu, Chunming He, Hao Wang, Hu Zhu, and Weiping Ding. Dm-fusion: Deep model-driven network for heterogeneous image fusion. *IEEE Transactions on Neural Networks and Learning Systems*, 2023. 9
- [57] Xiaogang Xu, Ruixing Wang, Chi-Wing Fu, and Jiaya Jia. Snr-aware low-light image enhancement. In *CVPR*, pages 17714–17724, 2022. 1, 5, 7, 8
- [58] Xiaogang Xu, Ruixing Wang, and Jiangbo Lu. Low-light image enhancement via structure modeling and guidance. In *CVPR*, pages 9893–9903, 2023. 5
- [59] Miao Yang and Arcot Sowmya. An underwater color image quality evaluation metric. *IEEE Transactions on Image Processing*, 24(12):6062–6071, 2015. 7

- [60] Wenhan Yang, Shiqi Wang, Yuming Fang, Yue Wang, and Jiaying Liu. Band representation-based semi-supervised low-light image enhancement: Bridging the gap between signal fidelity and perceptual quality. *IEEE Transactions on Image Processing*, 30:3461–3473, 2021. [5](#)
- [61] Wenhan Yang, Wenjing Wang, Haofeng Huang, Shiqi Wang, and Jiaying Liu. Sparse gradient regularized deep retinex network for robust low-light image enhancement. *IEEE Transactions on Image Processing*, 30:2072–2086, 2021. [1](#), [6](#)
- [62] Xunpeng Yi, Han Xu, Hao Zhang, Linfeng Tang, and Jiayi Ma. Diff-retinex: Rethinking low-light image enhancement with a generative diffusion model. In *ICCV*, pages 12302–12311, 2023. [1](#), [2](#), [3](#), [5](#), [6](#), [7](#)
- [63] Syed Waqas Zamir, Aditya Arora, Salman Khan, Munawar Hayat, Fahad Shahbaz Khan, and Ming-Hsuan Yang. Restormer: Efficient transformer for high-resolution image restoration. In *CVPR*, pages 5728–5739, 2022. [5](#), [7](#), [8](#)
- [64] Syed Waqas Zamir, Aditya Arora, Salman Khan, Munawar Hayat, Fahad Shahbaz Khan, Ming-Hsuan Yang, and Ling Shao. Learning enriched features for real image restoration and enhancement. In *ECCV*, pages 492–511. Springer, 2020. [5](#), [8](#)
- [65] Fan Zhang, Yu Li, Shaodi You, and Ying Fu. Learning temporal consistency for low light video enhancement from single images. In *CVPR*, pages 4967–4976, 2021. [8](#)
- [66] Richard Zhang, Phillip Isola, Alexei A Efros, Eli Shechtman, and Oliver Wang. The unreasonable effectiveness of deep features as a perceptual metric. In *CVPR*, pages 586–595, 2018. [7](#)
- [67] Yonghua Zhang, Jiawan Zhang, and Xiaojie Guo. Kindling the darkness: A practical low-light image enhancer. In *ACM MM*, pages 1632–1640, 2019. [8](#)
- [68] Naishan Zheng, Man Zhou, Yanmeng Dong, Xiangyu Rui, Jie Huang, Chongyi Li, and Feng Zhao. Empowering low-light image enhancer through customized learnable priors. In *ICCV*, pages 12559–12569, 2023. [5](#), [8](#)
- [69] Jingchun Zhou, Qian Liu, Qiuping Jiang, Wenqi Ren, Kin-Man Lam, and Weishi Zhang. Underwater camera: Improving visual perception via adaptive dark pixel prior and color correction. *International Journal of Computer Vision*, pages 1–19, 2023. [1](#), [7](#)